Spin Plane Control and Thrust Vectoring of Electric Solar Wind Sail by Tether Potential Modulation

Petri K. Toivanen[1] and Pekka Janhunen
Finnish Meteorological Institute, Helsinki, FIN-00560, Finland

The electric solar wind sail is a propulsion system that uses long centrifugally spanned and electrically charged tethers to extract the solar wind momentum for spacecraft thrust. The sail angle with respect to the sun direction can be controlled by modulating the voltage of each tether separately to produce net torque for attitude control and thrust vectoring. A solution for the voltage modulation that maintains any realistic sail angle under constant solar wind is obtained. Together with the adiabatic invariance of the angular momentum, the tether spin rate and coning angle is solved as functions of temporal changes in the solar wind dynamic pressure, the tether length, or the sail angle. The obtained modulation also gives an estimate for the fraction of sail performance (electron gun power) to be reserved for sail control. We also show that orbiting around the Sun with a fixed sail angle leads to a gradual increase (decrease) in the sail spin rate when spiraling outward (inward). This effect arises from the fact that the modulation of the electric sail force can only partially cancel the Coriolis effect, and the remaining component lays in the spin plane having a cumulative effect on the spin rate.

---

[1] Finnish Meteorological Institute, Earth Observation, P.O. Box 503, FIN-00101, Helsinki, Finland

Nomenclature

A = tether wire cross-sectional area

α = sail angle

$\mathbf{e}$ = unit vector

$\mathbf{F}$ = force

g = tether voltage modulation

I = tether moment of inertia

l = tether length

$\mathbf{L}$ = angular momentum

Λ = sail coning angle

m_p = proton mass

n_{w} = solar wind number density

$\boldsymbol{\omega}$ = angular velocity

$\widetilde{\omega}$ = angular frequency

$\boldsymbol{\Omega}$ = angular velocity of sail turning

P_{dyn} = solar wind dynamic pressure

(r, θ, φ) = spherical polar coordinates

ρ_l = tether material linear mass density

ρ_V = tether material mass density

T = tether root tension

$\boldsymbol{\tau}$ = torque

$(\theta_{\mathrm{w}}, \varphi_{\mathrm{w}})$ = solar zenith angles

$\mathbf{u}$ = solar wind velocity

V = tether voltage

$\mathbf{v}$ = velocity

I. Introduction

The electric solar wind sail was proposed in [1] as a propulsion system that uses the ambient interplanetary solar wind momentum flux for spacecraft thrust as inspired by the earlier magnetic sail concept in [2]. The proposed electric sail consisted of a conducting mesh charged to a high positive potential to repel the solar wind ions. Later, it was recognized that centrifugally stretched micro-meteoroid resistant tethers [3] can be used to construct the sail [4, 5]. It was noticed that an electric field potential structure of the spatial range larger than 100 m can be created around a thin wire with thickness of a few tens of micrometers. While such a construction provided a lightweight sail with an effective area comparable to a mesh, it also suggested a convenient way both to open the sail in space by reeling out the tethers instead of unfolding the mesh and also to control the sail spin plane by modulating the voltage of the electrically independent tethers.

The flight attitude control of a single tether and collectively the sail is a key challenge in electric sail development. Recently, it was shown that if attitude control is accomplished, the navigation in real solar wind conditions to planetary targets with an electric sail is feasible [6]. The sail inclination with respect to the sun-direction can be controlled and altered by modulating the individual tether voltage synchronously with the sail rotation, resembling helicopter flight from the algorithmic point of view. Since the tethers are much longer (up to tens of kilometers) than any realistic spacecraft radius, the rotation phase of the tether is not stabilized by the centrifugal force as is the case for the helicopter blades attached to the central plate. Initially, it was envisioned that the individual tether rotation rate can be controlled by varying the tether length by reeling. This would necessitate mechanical moving bodies, and as a more attractive option, auxiliary tethers connecting the tether tips can be added for mechanical stability to the baseline configuration [7].

The existing thrust law for an infinitely long positively charged electric sail tether is based on the studies in [5] and [8]. In general, the thrust force is proportional to the solar wind dynamic pressure and the effective area of the sail and its direction is along the component of the solar wind that is perpendicular to the tether. The latter feature is a key difference in comparison with the solar sail for which the thrust is perpendicular to the sail surface (assuming fully reflecting sail material). Since the tether voltage is much higher than the electron temperature, the Debye

length is not necessarily the scale size of the tether potential structure. Initially, a particle-in-cell computer simulation was used to predict the thrust law [5]. Based on these simulation results, the potential structure scale size is of the order of hundred meters. Later, it was noted that due to the complex electric field structures near the spacecraft, the electron motion becomes chaotic and the electrons trapped by the wire will be scattered [8]. Such a mechanism effectively removes the trapped electrons. This is, however, difficult to take into account self-consistently in the original simulation, and an analytical solution for the thrust law was constructed in [8]. It was argued that the analytic solution is in good agreement both with the simulation results (except that the thrust is about 5 times larger than that based on the simulations) and with the study by [9]. Concerning the present work, since the rotation rate of the sail is a free parameter, possible ambiguities of the thrust law do not invalidate the results of this paper that depend only on the ratio of the electric sail and centrifugal forces, i.e., the coning angle of the sail.

The electric sail tether dynamics and control includes a rotating body in a frame of reference rotating along with the sail orbiting around the Sun and introducing effects to the tether rotation period not necessarily intuitive in the framework of a freely swinging spherical pendulum. In Section 2, we introduce the electric sail thrust law together with coordinate systems to derive the single tether equation of motion. At this stage, it is adequate to consider a single tether as the Coulomb interaction between the tethers is weak due to the plasma shielding of the tether potential structures. An analytic solution for the tether voltage modulation for any tether spin plane orientation relevant for sail operations is obtained in Section 3 where we also give examples of variation in electric sail force and tether length tuning. The Coriolis effect is considered in Section 4 and examples of turning of the sail spin plane together with the result of the sail spin period evolution with controlled orbiting around the Sun are shown. In Sections 3 and 4, we give both the exact analytic solutions and their approximations for small coning angles. The results and implications to electric sail control and performance are summarized in Section 5. Limitations of the tether model used in this paper are also discussed in terms of realistic flexible tethers and variable solar wind conditions.

II. Electric sail tether motion

A. Thrust law

The magnitude of the force per tether length is given in [7] as

$$\frac{dF_u}{dz} \approx 0.18 \max(0, V - V_{\rm w})\sqrt{\epsilon_0 P_{\rm dyn}}, \tag{1}$$

where V is the tether voltage, $V_{\rm w}$ is the electric potential ($m_p u^2/2e$) corresponding to the kinetic energy of the solar wind ions, and $P_{\rm dyn}$ is the dynamic pressure of the solar wind, $P_{\rm dyn} = m_p n_{\rm w} u^2$. In Equation (1), $n_{\rm w}$ and u are the solar wind number density and flow speed, respectively. As the force exerted to the tether by the solar wind is perpendicular to the tether, the tether thrust vector is written as

$$\frac{d\mathbf{F}_u}{dz} = \xi \mathbf{u}_\perp, \tag{2}$$

where $\xi = 0.18 \max(0, V - V_{\rm w})\sqrt{\epsilon_0 m_p n_{\rm w}}$. Concerning the results of this paper, the exact value of ξ is not critical. The sail spin period is a free parameter that can be adapted so that the solar wind force is a desirable fraction of the tether centrifugal force corresponding to the tangent of the tether coning angle (Figure 1b) that defines the sail dynamics. The electric sail thrust integrated over the sail tethers points approximately to the median direction ($\mathbf{f}_u$) of the solar wind ($\mathbf{u}$) and sail normal ($\mathbf{n}$) directions as shown in Figure1a. This is a difference between the electric sail and the photon sail for which the thrust is normal to the sail surface.

B. Coordinate systems

For further analysis, we define two coordinate systems. Both systems are sail-centric with the Y axis being perpendicular to the solar ecliptic plane. The one shown in Fig 1a, the Sail-centric Solar Ecliptic (SSE) system has the Z axis pointing to the Sun, and the X axis completing the right handed triad. The other, the Sail Ecliptic (SE) system (Fig 1b) is obtained by rotating the SSE coordinates by the sail angle (α) with respect to the Y axis. As implied by the name, the SSE system is analogous to the Geocentric Solar Ecliptic (GSE) system, except that $X_{\rm SSE}$ = -$Y_{\rm GSE}$, $Y_{\rm SSE}$ = -$Z_{\rm GSE}$, and $Z_{\rm SSE}$ = $X_{\rm GSE}$. Note that the definition of these coordinate systems in traditional terms of the ecliptic plane is arbitrary, and the ecliptic plane can also be considered as the sailcraft orbital plane.

The analysis of the temporal evolution of the tether key variables, coning angle and rotation rate, is simplest in the spherical SE coordinates as the desired sail orientation corresponds to the solution of constant polar angle ($\dot{\theta}_{\mathrm{SE}} = 0$). Since the SE system is not inertial, fictitious forces arising from the Coriolis

$$\mathbf{F}_C = -2m\,\boldsymbol{\Omega} \times \mathbf{v}, \tag{3}$$

centripetal ($\mathbf{F}_{cp} = -m\,\boldsymbol{\Omega} \times (\boldsymbol{\Omega} \times \mathbf{r})$), and Euler ($\mathbf{F}_E = -m\,\dot{\boldsymbol{\Omega}} \times \mathbf{r}$) effects have to be taken into account. In general, $\mathbf{r}$ and $\mathbf{v}$ are the particle position and velocity vectors in a reference frame rotating with an angular velocity vector $\boldsymbol{\Omega}$. In this study, $\boldsymbol{\Omega}$ is determined either by the turning of the sail spin plane or by the orbital motion around the Sun. Since the angular frequency of the sail rotation is much higher than that of the SE system, the centripetal and Euler effects can be neglected as being of the second order in Ω.

C. Equation of motion

The equation of the tether motion can be obtained from

$$\frac{d\mathbf{L}}{dt} = \frac{d}{dt}\left(I\boldsymbol{\omega}\right) = \boldsymbol{\tau}_{\mathrm{w}} + \boldsymbol{\tau}_C \tag{4}$$

as expressed in terms of the tether angular momentum ($\mathbf{L}$), angular velocity ($\boldsymbol{\omega}$), the moment of inertia (I), and torques arising from the electric sail force ($\boldsymbol{\tau}_{\mathrm{w}}$) and Coriolis effect ($\boldsymbol{\tau}_{\mathrm{C}}$). For a thin tether wire,

$$I = \frac{1}{3}\rho_V A l^3, \tag{5}$$

where ρ_V is the mass density of the tether material, A is the cross-sectional area of the wire, and l is the tether length. Using Equation (2), $\boldsymbol{\tau}_{\mathrm{w}}$ is integrated over the tether length as

$$\begin{aligned} \boldsymbol{\tau}_{\mathrm{w}} &= \int_0^l \mathbf{r} \times d\mathbf{F}_{\mathrm{u}} \\ &= \frac{1}{2}\xi l^2(-u_\varphi \mathbf{e}_\theta + u_\theta \mathbf{e}_\varphi), \end{aligned} \tag{6}$$

where

$$\begin{aligned} u_\theta &= u_x \cos\theta\cos\varphi + u_y \cos\theta \sin\varphi - u_z \sin\theta \\ u_\varphi &= -u_x \cos\varphi + u_y \cos\varphi \end{aligned} \tag{7}$$

are the spherical components of the solar wind, and l is the tether length. Defining the tether velocity in spherical coordinates, the torque caused by the Coriolis effect (3) can be integrated over the tether length as in (6) as

$$\begin{aligned} \boldsymbol{\tau}_C &= \int_0^l 2\rho_l(\mathbf{r}\cdot\boldsymbol{\Omega})\mathbf{v}dr \\ &= 2I\Omega\sin\theta\sin\varphi(\dot{\theta}\mathbf{e}_\theta + \sin\theta\dot{\varphi}\mathbf{e}_\varphi), \end{aligned} \tag{8}$$

where any terms including possible tether length time variation have been neglected, and ρ_l is the tether mass per unit length. Here, we assumed that the sail is orbiting on the ecliptic plane and tilted as shown in Figure 1a, and $\boldsymbol{\Omega} = \Omega\mathbf{e}_y$. The angular velocity in Equation (4) can be solved from $\mathbf{v} = \boldsymbol{\omega}\times\mathbf{r}$ to read as

$$\boldsymbol{\omega} = -\sin\theta\dot{\varphi}\mathbf{e}_\theta + \dot{\theta}\mathbf{e}_\varphi. \tag{9}$$

For further manipulation of the equation of motion (4), we express the solar wind velocity in terms of the zenith angles of its nominal direction (θ_w and φ_w) as

$$\begin{aligned} u_\theta &= u\left(\sin\theta_\mathrm{w}\cos\theta\cos(\varphi-\varphi_\mathrm{w}) - \cos\theta_\mathrm{w}\sin\theta\right) \\ u_\varphi &= -u\sin\theta_\mathrm{w}\sin(\varphi-\varphi_\mathrm{w}) \end{aligned} \tag{10}$$

defined by

$$\begin{aligned} u_x &= u\sin\theta_\mathrm{w}\cos\varphi_\mathrm{w} \\ u_y &= u\sin\theta_\mathrm{w}\sin\varphi_\mathrm{w} \\ u_z &= u\cos\theta_\mathrm{w}. \end{aligned} \tag{11}$$

For completeness of the equation of motion, the solar wind zenith phase angle is explicitly left here although $\varphi_\mathrm{w} = 0$ for the case considered in this study. After these definitions, taking the time derivative and rearranging the spherical vector components, we write the equation of motion as

$$\begin{aligned} l^3\sin\theta\cos\theta\,\dot{\varphi}^2 &= -g\lambda l^2\left(\sin\theta_\mathrm{w}\cos\theta\cos(\varphi-\varphi_\mathrm{w}) - \cos\theta_\mathrm{w}\sin\theta\right) \\ &\quad -2\Omega l^3\sin^2\theta\sin\varphi\dot{\varphi} \\ &\quad +\frac{d}{dt}\left(l^3\dot{\theta}\right) \end{aligned} \tag{12}$$

$$\frac{d}{dt}\left(l^3\sin^2\theta\dot{\varphi}\right) = -g\lambda l^2\sin\theta_{\rm w}\sin\theta\sin\varphi$$
$$+2\Omega l^3\sin^2\theta\sin\varphi\dot{\theta}, \tag{13}$$

where

$$\lambda = \frac{3\xi u}{2\rho_l}. \tag{14}$$

In Equations (12) and (13) we have explicitly added the tether voltage modulation g. In addition to the tether key variables, it is important to consider the tension at the root of the tether as

$$T = \rho_V\left(\frac{1}{2}l^2\left(\dot{\theta}^2+\sin^2\theta\dot{\varphi}^2\right)-\frac{d}{dt}\left(l\dot{l}\right)\right) \tag{15}$$

for the diagnostics. While the equation of motion (12 and 13) is written for an arbitrary solar wind direction including also possible non-radial components, the rest of the paper deals with a constant solar wind and sail orbit on the ecliptic plane, and $\theta_{\rm w}=\alpha$ and $\varphi_{\rm w}=0$.

III. Solution for fixed tether spin plane ($\Omega = 0$)

In general, the tether attitude control can be addressed by the tether voltage modulation g introduced in the equation of motion (12) and (13). The tether spin plane can then be fixed to correspond to any relevant sail pointing angle with a voltage modulation that attempts to maintain $\dot{\theta}$ at zero in SE coordinates (Figure 1b). This can be done either numerically ($g=g_n$) or analytically ($g=g_a$). In the former case, the modulation can be realized by a linear controller

$$g_n = 1+c_n\dot{\theta} \tag{16}$$

that monitors the latitudinal speed $\dot{\theta}$ and corrects the tether voltage if $\dot{\theta}$ deviates from zero. For constant solar wind, an analytic form for the modulation exists depending only on the tether rotation phase: Inserting a modulation of

$$g_a(\varphi) = c_a\left(\sin\alpha\cos\theta\cos\varphi-\cos\alpha\sin\theta\right)^{-3} \tag{17}$$

in the equation of motion (12) and(13), it can be seen that $\dot{\theta}=0$. The constant c_a can be fixed by normalizing the angular average of $g_a(\varphi)$ to unity,

$$< g_a(\varphi) >_\varphi = \frac{1}{2\pi}\int_0^{2\pi} g(\varphi)d\varphi = 1. \tag{18}$$

The integral has a closed form and can be determined by partial integration. After this normalization, the modulation can be written as

$$g_a(\varphi) = \frac{2\left(1-\chi^2\right)^{5/2}}{\left(2+\chi^2\right)\left(1+\chi\cos\varphi\right)^3} \tag{19}$$

$$\approx 1 - 3\chi\cos\varphi + \mathcal{O}(\tan^2\Lambda), \tag{20}$$

where $\chi = \tan\alpha\tan\Lambda$, and the approximation (20) is for small coning angles. When considering the voltage source design of the electric sail, (19) implies that the voltage has to include design margin by a factor of

$$\max(g_a(\varphi)) = \frac{2\left(1-\chi^2\right)^{5/2}}{\left(2+\chi^2\right)\left(1-|\chi|\right)^3} \tag{21}$$

reserved for the modulator (Figure 2). It can be concluded that the larger the sail angle and the coning angle (slower spin rate) are the larger amplitude modulation is needed for the tether control.

Applying the analytic modulation (19) in Equations (12) and (13), it can be shown that the coning angle (Λ) depends on the average angular frequency ($\widetilde{\omega} =< \dot{\varphi} >_\varphi$) as

$$\widetilde{\omega}^2 = \frac{2\lambda\cos\alpha\left(1-\chi^2\right)^{3/2}}{l\sin\Lambda\left(2+\chi^2\right)} \tag{22}$$

$$\approx \frac{\lambda\cos\alpha}{l\sin\Lambda}\left(1+\mathcal{O}(\tan^2\Lambda)\right). \tag{23}$$

Taking angular average of (13), it can be seen that

$$\frac{d}{dt}\left(l^3\widetilde{\omega}\cos^2\Lambda\right) = 0 \tag{24}$$

$$\frac{d}{dt}\left(l^3\widetilde{\omega}\right) \approx \mathcal{O}(\tan^2\Lambda) \tag{25}$$

implying that $l^3\widetilde{\omega}\cos^2\Lambda$ is an adiabatic invariant of motion. Using Equations (22) and (24), $\widetilde{\omega}$ and Λ can be solved as functions of time corresponding to a given temporal change of λ and l as shown in examples below.

A. Example: Variations in electric sail force

Variations in the electric sail force are caused by the tether voltage or solar wind conditions. Using Equations (22) and (24), the coning angle and angular frequency can be solved as functions of the relative electric sail force (λ/λ_0) as shown in Figures 3a and 3b, respectively. The curves shown

are for five initial coning angles ranging from 2° to 10° spaced by 2 degrees. Based on (24) for a constant tether length, the force variations have relatively weak effect on the angular frequency.

B. Example: Tether length tuning

The tether length tuning can be used to vary the tether rotation rate as predicted by (22) and (24). Figure 4 shows the coning angle and angular frequency as functions of the tether length (l) relative to the initial length (l_0). These are shown for five initial coning angles ranging from 2° to 10° spaced by 2 degrees. As implied by Figure (4b), the approximate (25) holds well and

$$\widetilde{\omega} = \widetilde{\omega}_0 \left(\frac{l_0}{l}\right)^3. \tag{26}$$

IV. Solution for rotating tether spin plane ($\Omega \neq 0$)

Solving the equation of motion (12) and (13) for a non-zero $\Omega << \widetilde{\omega}$, assumes an additional variation (δg) in the voltage modulation, $g \to g + \delta g$ with $\delta g << g$. Inserting such a modulation in (12) and using (22), δg as a function of the phase angle can be written as

$$\delta g = -\frac{2\Omega l \widetilde{\omega} \sin\theta \sin\varphi}{\lambda \cos\alpha \,(1 + \chi \cos\varphi)}. \tag{27}$$

Inserting δg in (13) and considering only angular averaged quantities, the time variation of the angular momentum is written as

$$\begin{aligned} \frac{d}{dt}\left(l^3 \widetilde{\omega} \cos^2\Lambda\right) &= 2l^3 \Omega \widetilde{\omega} \tan\alpha \cos^2\Lambda \left\langle \frac{\sin^2\varphi}{(1+\chi\cos\varphi)} \right\rangle_\varphi \\ &\approx l^3 \Omega \widetilde{\omega} \tan\alpha \cos^2\Lambda + \mathcal{O}(\tan^2\Lambda) \end{aligned} \tag{28}$$

after expanding $(1 + \chi\cos\varphi)^{-1}$ in χ, noting that $< \sin^2\varphi >_\varphi = 1/2$, and $< \sin^2\varphi \cos\varphi >_\varphi = 0$.

A. Example: Turning of the sail spin plane

Figure 5 shows a controlled turn of the sail spin plane with the initial sail angle changing from $\alpha = 0°$ to $\alpha = 45°$ as a function of time $\alpha(t)$ as shown in Figure 6a. This steering signal is then used to alter the reference signal (19) of the voltage modulation. Finally, the tether variables are transformed to the system rotated by $\alpha(t)$ and the control (16) applied in the rotated frame. Note that the sail can be turned to any orientation ($\varphi_w \neq 0$) by using the tether phase as another steering

signal to feed the reference modulation. The voltage modulation combining both the reference and the control signals is shown in Figure 6b.

Analytically, based on Equation (28), the turning of the sail can be considered as follows. By definition, $\Omega = \dot{\alpha}$, and it can be seen that

$$\frac{d}{dt}\left(l^3\widetilde{\omega}\cos^2\Lambda\cos\alpha\right) = 0 \tag{29}$$

$$\frac{d}{dt}\left(l^3\widetilde{\omega}\cos\alpha\right) \approx \mathcal{O}(\tan^2\Lambda) \tag{30}$$

as written in terms of the coning angle Λ. Hence, $l^3\widetilde{\omega}\cos^2\Lambda\cos\alpha$ is an adiabatic invariant, and any changes of the sail primary variables $\widetilde{\omega}$ and Λ in the sail angle maneuvers can be determined by using (22) and (29). The adiabatic invariant scaled to its initial value, μ is shown in Figure 6c as determined by the tether variables. Using Equations (23) and (30), the time variation of the tether coning angle and angular frequency can be solved following well the actual time evolution (black solid line) as shown by gray dashed lines in Figures 6d and 6e, respectively. Finally, the tether root tension scaled to the tensile strength of aluminum is shown in Figure 6f.

In general, using Equations (22) and (29), the coning angle (Figure 7a) and the angular frequency (Figure 7b) can be solved as functions of the sail angle. As an estimate, the angular frequency depends on the sail angle as

$$\widetilde{\omega} = \widetilde{\omega}_0\left(\frac{\cos\alpha_0}{\cos\alpha}\right) \tag{31}$$

holding well for the relevant sail angles. The result implies that the amount of the initial angular momentum can be reduced by starting the sail rotation with the sail pointing to the Sun and then turning the sail as shown in Figure 5 to a desired inclination with respect to the Sun. In addition to the tether reeling shown in Figure 4, the tether angular frequency can also be altered by changing the tether angle.

B. Example: Maintaining the sail angle on orbit

The sail angle dependence of the sail spin rate has an important implication on the electric sail dynamics when orbiting around the Sun. As the sail spin plane maintains it orientation with respect to the distant stars (Figure 8a), the sail angle is slowly ($\sim 1^\circ$ per day) changing and the sail

is rotating in the SSE coordinate system along the orbit around the Sun. Equivalently, the rotation can be associated with a weak Coriolis force acting on the tether in SSE. However, to produce constant thrust, the sail angle has to be fixed with respect to the Sun direction. This can be done by the modulation of the electric sail force as depicted in Figures 8b and 8c.

In Figure 8b, the tether tip is on the spin plane (dashed line) at (X_{SSE} =Z_{SSE} = 0) pointing downward (Y_{SSE} = l). Since the SSE system is rotating with $\mathbf{\Omega}$ being anti-parallel to the Y_{SSE} axis, the Coriolis force ($\mathbf{F}_C \propto \mathbf{v} \times \mathbf{\Omega}$) is normal to the sail spin plane. However, as the electric sail force is always aligned with the sun-sail line, only the corresponding component of $\mathbf{F}_C$ can be canceled by the sail force modulation ($\mathbf{F}_{\rm ES}$). While such a modulation maintains the sail attitude with respect to the sun-sail line, the resultant force ($\mathbf{F}_{\rm ES}^{\perp}$) has a component in the direction of the tether tip velocity ($\mathbf{v}$). As this is the case also with the upward orientation of the tether (Figure 8b), the spin rate of the sail slowly increases for positive sail angles (orbiting away from the Sun). For a negative sail angle (spiraling towards the Sun), the spin rate is expected to decrease.

Although this effect may well be negligible in the time scale of the sail rotation periods, the accumulated change in the spin rate has to be taken into account for typical mission time scales. Mathematically, the considerations above are included in Equation (28) for coning angles typical for an electric sail. Now, $\Omega = 2\pi$/year corresponding to the slow rotation of the SSE system along the orbit around the sun. Since the sail angle is kept constant ($\dot{\alpha} = 0$), Equation (28) leads to an differential equation for $\widetilde{\omega}\cos^2\Lambda$ that can easily be solved as

$$\begin{aligned} \widetilde{\omega}\cos^2\Lambda &= \widetilde{\omega}_0\cos^2\Lambda_0 e^{\Omega\tan\alpha(t-t_0)}. \\ \widetilde{\omega} &\approx \widetilde{\omega}_0 e^{\Omega\tan\alpha(t-t_0)} + \mathcal{O}(\tan^2\Lambda). \end{aligned} \tag{32}$$

If the sail angle is negative (positive) and the sail is orbiting towards (away from) the Sun, the spin rate decreases (increases). Figure 9 shows the key sail parameters as a function of time for an time interval of 50 days. These are shown for two sail angles of $\pm 45°$. The voltage modulation (Figure 9a) shows vastly different behavior depending on the sign of the sail angle as expected by Figure 2: For the positive (negative) sail angle, the tether coning angle decreases (increases) while the spin rate increases (decreases). It can be concluded that Equation (32) compares well with the numerical results, and the accumulated changes in the spin rate are significant in terms of mission time scales.

V. Conclusions

The results of this paper are based on a simple dynamical model for the electric sail tether, a spherical pendulum rotating under constant solar wind forcing. This model assumes that the tether is straight, i.e., well tightened by the centrifugal force. We derived rules for the electric sail tether dynamics and control in terms of the key tether variables, coning angle and spin rate. The analysis also provided us with an estimation of the voltage (and thus power) overhead to be reserved for tether control. The amount of overhead depends on the coning angle, implying that a slowly spinning sail requires more voltage reserve for its control than a fast spinning sail. The key variables depend mainly on the exerted electric sail force (tether voltage and solar wind dynamic pressure), tether length, and tether angle. Changes in the electric sail force lead to only minor changes in the tether spin rate while changes in the sail configuration (tether length) and orientation (for typical sail angles) have a major effect on the tether spin rate. This is practical since for a given flight configuration and orientation, the sail spin rate differs moderately from the spacecraft spin rate due to the solar wind variations.

In addition, we described an non-trivial effect of the gradually evolving spin rate arising from the sail orbital motion around the Sun and the related Coriolis effect. The tether voltage modulation can be used to cancel the component of the Coriolis force normal to the sail spin plane and thus maintain the electric sail orientation with respect to the sun-direction. However, the remaining component lies in the spin plane, leading to a cumulative decrease or increase of the sail spin rate for negative (inward) and positive (outward) sail angles, respectively. The reason for this effect is that the electric sail force is not normal to the sail spin plane. Our analytical results showed that the magnitude of the effect is such that it has to be taken into account in typical mission scenarios. While it may somewhat complicate electric sail mission design, a possibility arises that the spin-up angular momentum for the sail deployment could be partly obtained by this effect. Furthermore, a clever control algorithm might be able to mitigate or nullify this effect by utilizing the natural small directional variations of the solar wind.

In this paper we did not consider the effects of the natural solar wind variations. It is likely that when these variations are taken into account, the bare electric sail model consisting only of

tethers and their individual potential control is not able to keep the tethers apart from each other and at the wanted tether angle at the same time. This is because each tether has two degrees of freedom (e.g., the tether angle and the phase angle) while the potential adjustment provides only one control parameter. Therefore it may well be that the electric sail design has to be augmented by some mechanism which keeps the tethers apart, such as auxiliary tethers connecting together the main tether tips [7] or small auxiliary propulsive devices (e.g. solar sails) at the tether tips. Even in the presence of such devices, however, it is beneficial if the applied potential control algorithm is such that it keeps the tethers moving approximately in the right way already by itself. Therefore we consider the bare electric sail model as a useful benchmarking arrangement when developing the potential control algorithm.

Acknowledgments

This work was supported by Academy of Finland.

References

[1] Janhunen, P., "Electric sail for spacecraft propulsion," *J. Propul. Power*, 20(4), 763–764, 2004.

[2] Zubrin, R. M., and Andrews, D. G., "Magnetic sails and interplanetary travel," *J. Spacecraft Rockets*, Vol. 28, 197–203, 1991.

[3] Hoyt, R., and Forward, R. L., U.S. Patent No. 6,286,788 B1, 2001.

[4] Janhunen, P., U.S. Patent No. 7,641,151, 2010.

[5] Janhunen, P., and Sandroos, A., "Simulation study of solar wind push on a charged wire: basis of solar wind electric sail propulsion," *Ann. Geophys.*, Vol. 25, 755–767, 2007.

[6] Toivanen, P. K., and Janhunen, P., "Electric sailing under observed solar wind conditions," *Astrophys. Space Sci. Trans.*, Vol. 5, 61–69, 2009.

[7] Janhunen, P., Toivanen, P. K., Polkko, J., Merikallio, S., Salminen, P., Haegström, E., Seppänen, H., Kurppa, r., Ukkonen, J., Kiprich, S., Thornell, G., Kratz, H., Richter, L., Krömer, O., Rosta, R., Noorma, M., Envall, J., Lätt, S., Mengali, G., Quarta, A. A., Koivisto, H., Tarvainen, O., Kalvas, T., Kauppinen, J., Nuottajärvi, A., and Obraztsov, A., "Electric solar wind sail: Towards test missions," *Rev. Sci. Instrum.*, Vol. 81, 111301, 2010.

[8] Janhunen, P., "Increased electric sail thrust through removal of the trapped shielding electrons by orbit chaotisation due to spacecraft body", *Ann. Geophys.*, Vol. 27, 3089–3100, 2009.

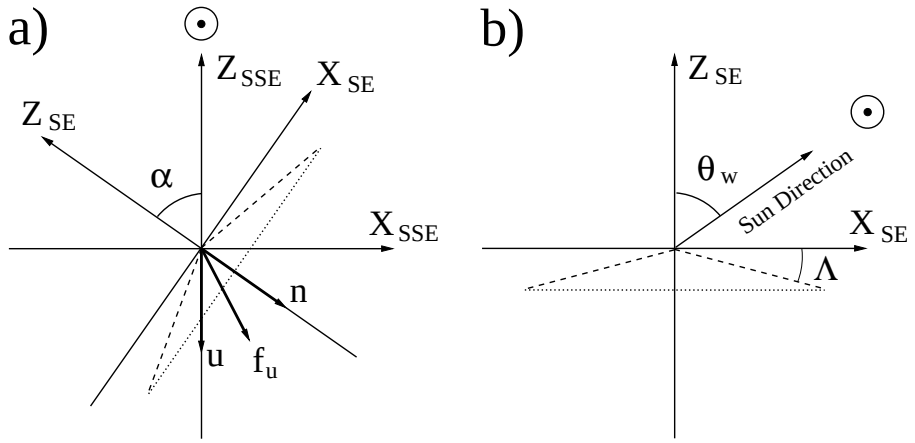

Fig. 1 Coordinate systems of (a) Sail-centric Solar Ecliptic (SSE) and (b) Sail Ecliptic (SE).

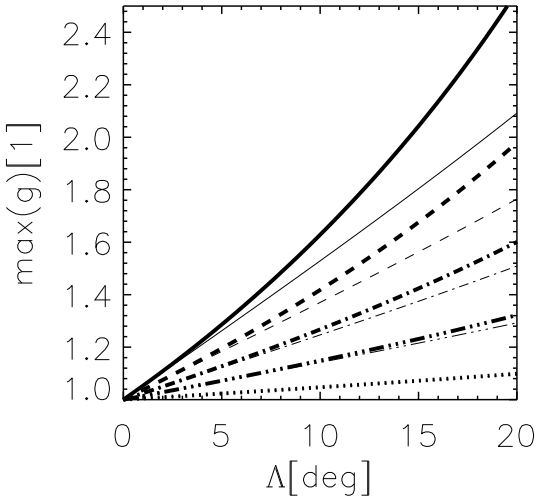

Fig. 2 Maximum of the control reference signal as a function of the coning angle as shown for five sail angles from 5° (thick dotted line) to 45° (thick solid line) with a spacing of 10°. The corresponding thin lines show the approximation for small coning angles.

[9] Sanmartín, J. R., Chroinière, E., Gilchrist, B. E., Ferry, J.-B., and Martínez-Sánchez, M., "Bare-tether sheath and current: comparison of asymptotic theory and kinetic simulations in stationary plasma," *IEEE Trans. Plasma Phys.*, Vol. 36, 2851–2858, 2008.

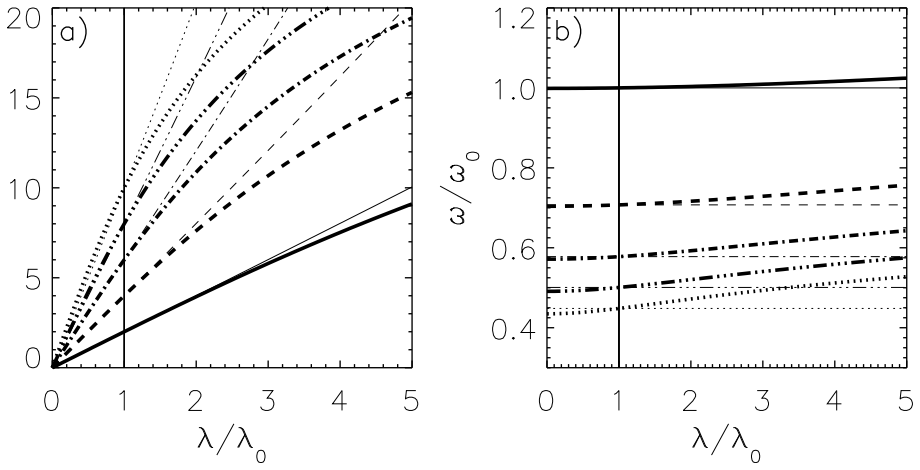

Fig. 3 (a) Coning angle and (b) relative angular frequency as functions of the electric sail force relative to a reference force. Both the adiabatic solution (thick) and its approximate for small coning angles (thin) are shown for five initial coning angles fixed at $\lambda/\lambda_0 = 1$.

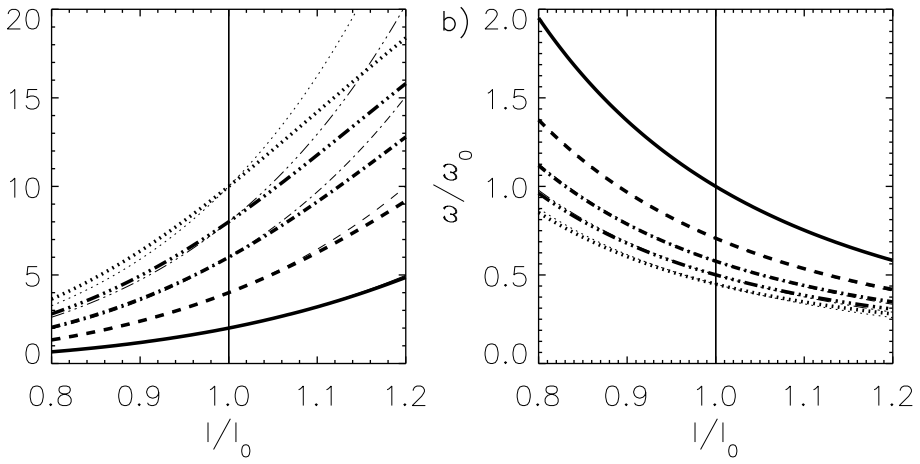

Fig. 4 (a) Coning angle and (b) relative angular frequency as functions of the tether length relative to a reference length. Both the adiabatic solution (thick) and its approximate for small coning angles (thin) are shown for five initial coning angles at $l/l_0 = 1$.

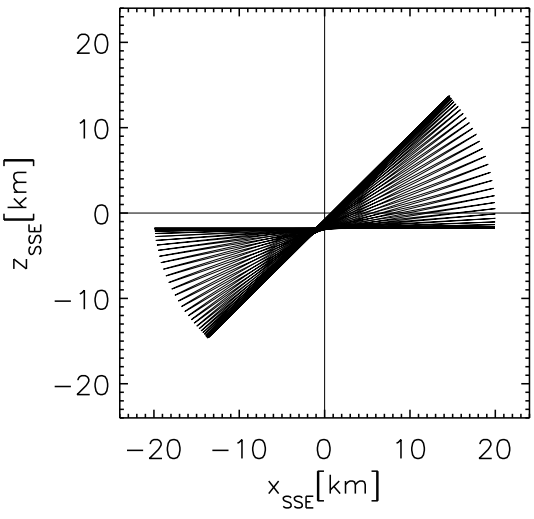

Fig. 5 Trace of the tether tip in SSE coordinates during a turning of the sail from an initial orientation with the sail angle of $\alpha = 0^\circ$ to $\alpha = 45^\circ$.

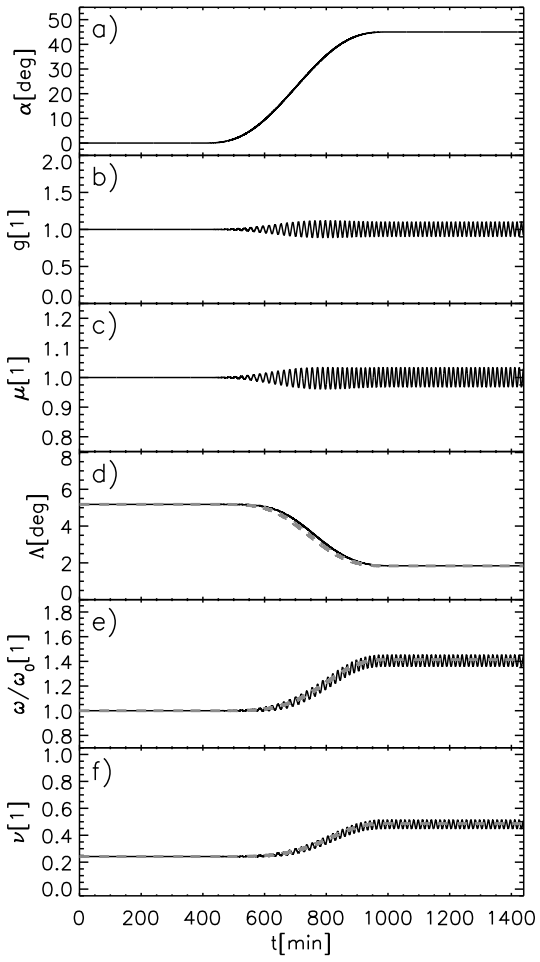

Fig. 6 Temporal evolution of the key sail variables during the sail spin plane turn shown in Figure 5, (a) sail angle, (b) tether modulation signal, (c) relative angular momentum, (d) coning angle, (e) relative angular frequency, and (f) tether root tension. The gray dashed curves show the result of the adiabatic approximation.

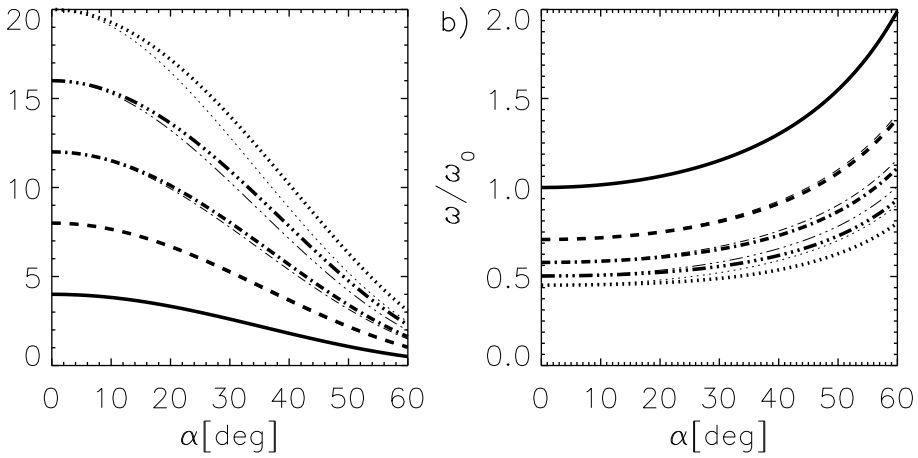

Fig. 7 (a) Coning angle and (b) relative angular frequency as a function of the sail angle. Both the adiabatic solution (thick) and its approximate for small coning angles (thin) are shown for five initial coning angles fixed at $\alpha = 0$.

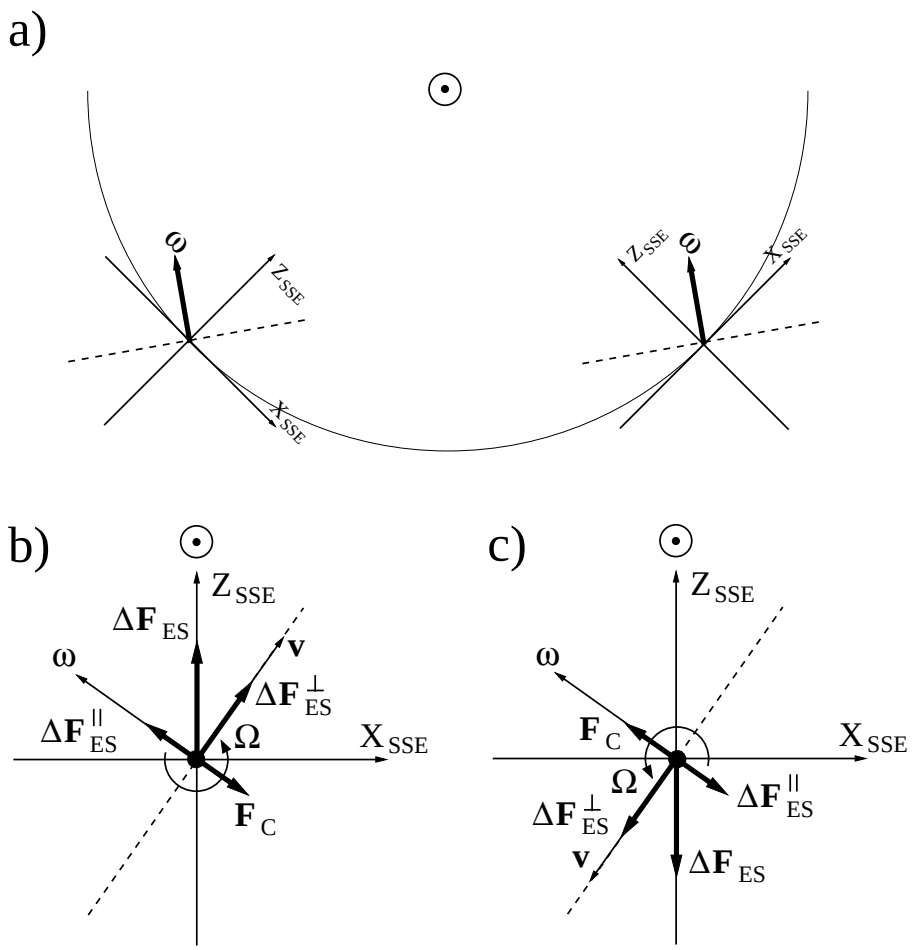

Fig. 8 (a) Sail spin plane (dashed line) orientation with respect to the distant stars and to the SSE system while orbiting around the Sun with no spin plane control applied. Orientations of the Coriolis force ($\mathbf{F}_C \propto -\mathbf{\Omega} \times \mathbf{v}$) acting on the tether pointing (b) anti-parallel and (c) parallel to the Y_{SSE} axis. The sail spin plane can be fixed with respect to the sun direction (positive sail angle shown) by modulation of the electric sail force ($\Delta\mathbf{F}_{ES}$) that cancels the Coriolis force ($\mathbf{F}_C$) aligned with the sail spin axis. However, the resultant force ($\Delta\mathbf{F}_{ES}^{\perp}$) is in the direction of the tether velocity (v) leading to a gradual increase in the tether spin rate in the case of the positive sail angle (the sail is orbiting outward). For a negative sail angle (orbiting inward), the spin rate is decreased (not shown).

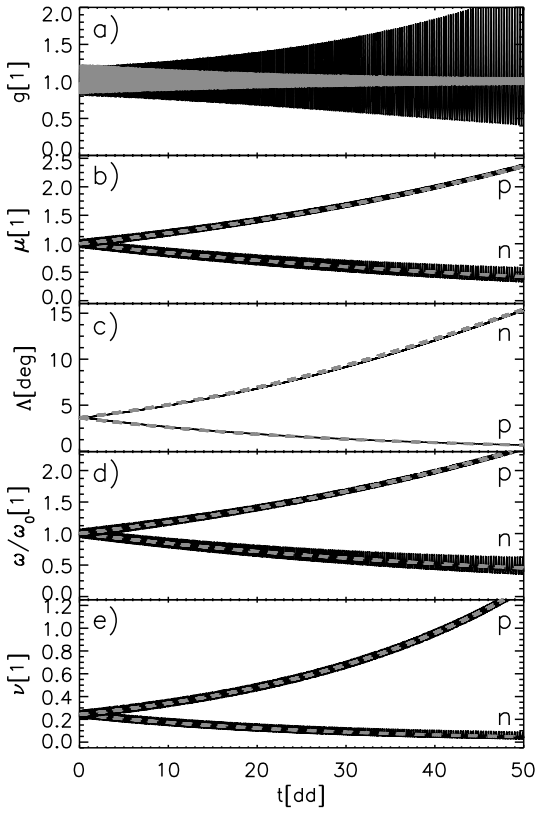

Fig. 9 Temporal evolution of the key sail variables during 50 days while orbiting around the Sun as shown for both the positive and negative sail angles: (a) Tether voltage modulation for positive (black) and negative (gray) sail angles, (b) relative angular momentum, (c) coning angle, (d) relative angular frequency, and (e) tether root tension. The black lines show the result of the numerical computations, and the dashed gray lines show the result of the analytical calculations for the positive (p) and negative (n) sail angles.